

Metallic State of the Three-band Hubbard Model with Super-lattice Structure

Shigeru Koikegami¹ * , Takashi Yanagisawa¹, and Masaru Kato²

¹*Nanoelectronics Research Institute, AIST Tsukuba Central 2, Tsukuba 305-8568, Japan*

²*Department of Mathematical Sciences, Osaka Prefecture University, Sakai 599-8531, Japan*

(Received January 27, 2006)

We investigate the dynamical superlattice correlation in the two-dimensional three-band Hubbard model on the basis of the unrestricted fluctuation exchange approximation. We calculate the one-particle spectral function, the spin correlation function and the charge correlation function at finite temperature. We find that some experimental results can be reproduced consistently by taking inhomogeneous distribution of Cu 3d electrons into account. The correlation functions suggest that several kinds of instabilities with spatial inhomogeneities exist in some regions, where these instabilities significantly affect the one-particle spectral functions.

KEYWORDS: super-lattice structure, unrestricted fluctuation exchange approximation, strong correlation effect, spatial inhomogeneity

1. Introduction

The quasi-one-dimensional (Q1D) charge order, which is well-known as the stripe order, has been one of the significant issues in high- T_c cuprates (HTC) for recent years. The incommensurate peaks observed by the neutron scattering in $\text{La}_{2-x}\text{Ba}_x\text{CuO}_4$ are to be explained on the assumption that the static stripe order is present around 1/8-filling.¹ The presence of the static stripe order in the ground state has been proved theoretically by the density matrix renormalization group method on the basis of the Q1D t - J model.² Originally, since the beginning of HTC studies many experimentalists have pointed out the so-called 1/8-problem in $\text{La}_{2-x}\text{Ba}_x\text{CuO}_4$, i.e., the remarkable suppression of superconducting transition temperature at $x \sim 1/8$. Many theorists have thought that the strong on-site Coulomb interaction makes electrons almost localized with the long-period spin and charge correlations around 1/8-filling. They have studied these long-period correlations by the numerical or analytical methods on the basis of the two-dimensional (2D) Hubbard models and have clarified that some long-period correlated states can be the ground states around certain fillings.³⁻¹² These theoretically predicted long-period correlation states are consistent with the stripe state deduced from the neutron scattering experiments.¹³

The theoretical results on the basis of the 2D Hubbard models mean that the strong

*E-mail: shigeru.koikegami@aist.go.jp

on-site interaction is enough to stabilize the stripe state near 1/8-filling as far as the ground state is considered. However, at finite temperature the strong fluctuations characteristic to the low dimensional strongly correlated electron systems exist. These strong fluctuations are composed of the many elements, e.g., the anti-ferromagnetic (AF) fluctuation and the charge ordering fluctuations with certain classes of super-lattice structures. These strong fluctuations accompany with the instabilities of the spin and charge orderings and simultaneously tend to interrupt them. The stripe with such strong fluctuations in metallic state is called a dynamical stripe.¹⁴⁻¹⁷ The angle resolved photo-emission spectroscopy (ARPES) shows that the stripes in $\text{Bi}_2\text{Sr}_2\text{CaCu}_2\text{O}_{8+\delta}$ has more dynamic character than those in $\text{La}_{2-x}\text{Sr}_x\text{CuO}_4$. The discrimination whether the stripe is static or dynamic is to be judged from the characteristic energy of the fluctuation mode. If the fluctuation mode has low characteristic energy, i.e., the stripe fluctuates slowly, the mode can easily couple with phonon and the static stripe long-range order will appear. On the other hand, if the fluctuation mode has high characteristic energy, i.e., the stripe fluctuates fast, the mode cannot couple with phonon and the system will stay metallic together with the fluctuation. When we consider these fluctuations in the analysis of these models without the long-ranged Coulomb interaction, we can expect that the metallic state should be recovered at higher temperature. In this state, however, the electronic property is to be still affected by the stripe instability as far as its dynamical factor is investigated

In this paper, we analyze the 2D three-band Hubbard model on the basis of the unrestricted fluctuation exchange approximation (UFLEX). UFLEX can consider a strong correlation effect and a number of the spatial inhomogeneities without any assumptions about the ground state. These considered effects contain not only a static component but a dynamic one. As a result, the electronic state reproduced on the basis of UFLEX is affected by a number of spatially inhomogeneous fluctuations simultaneously. In fact, when we calculate the one-particle spectral functions and the spin correlation functions for our fully self-consistent solutions, we can find that the one-particle spectra of the electronic state reflect these exotic state accompanied with the anti-ferromagnetic or the further long-periodic instabilities. Especially, near 1/8-filling the spin and charge correlation functions show the existence of the Q1D fluctuation at finite frequency. This fast Q1D fluctuation is originated from the striped spatial inhomogeneity. Thus, our results suggest that the spatial inhomogeneities should be concerned in the strongly correlated electron system when the electronic behavior at a finite frequency is discussed.

2. 2D three-band Hubbard model

Our 2D three-band Hubbard model Hamiltonian, H , is composed of d -electrons at each Cu site and p -electrons at O site. We consider only the on-site Coulomb repulsion U between d -electrons at each Cu site. Then, H is divided into the non-interacting part, H_0 , and the

interacting part, H_1 , as

$$H = H_0 + H_1 - \mu \sum_{\mathbf{k}\sigma} (d_{\mathbf{k}\sigma}^\dagger d_{\mathbf{k}\sigma} + p_{\mathbf{k}\sigma}^{x\dagger} p_{\mathbf{k}\sigma}^x + p_{\mathbf{k}\sigma}^{y\dagger} p_{\mathbf{k}\sigma}^y). \quad (1)$$

Here $d_{\mathbf{k}\sigma}$ ($d_{\mathbf{k}\sigma}^\dagger$) and $p_{\mathbf{k}\sigma}^{x(y)}$ ($p_{\mathbf{k}\sigma}^{x(y)\dagger}$) are the annihilation (creation) operator for p - and $p^{x(y)}$ -electron of momentum \mathbf{k} and spin σ , respectively. μ is the chemical potential. The non-interacting part H_0 is represented by

$$H_0 = \sum_{\mathbf{k}\sigma} \begin{pmatrix} d_{\mathbf{k}\sigma}^\dagger & p_{\mathbf{k}\sigma}^{x\dagger} & p_{\mathbf{k}\sigma}^{y\dagger} \end{pmatrix} \begin{pmatrix} \Delta_{dp} & \zeta_{\mathbf{k}}^x & \zeta_{\mathbf{k}}^y \\ -\zeta_{\mathbf{k}}^x & 0 & \zeta_{\mathbf{k}}^p \\ -\zeta_{\mathbf{k}}^y & \zeta_{\mathbf{k}}^p & 0 \end{pmatrix} \begin{pmatrix} d_{\mathbf{k}\sigma} \\ p_{\mathbf{k}\sigma}^x \\ p_{\mathbf{k}\sigma}^y \end{pmatrix}, \quad (2)$$

where Δ_{dp} is the hybridization gap energy between d - and p -orbitals. We take the lattice constant of the square lattice formed of Cu sites as the unit of length, and we can represent $\zeta_{\mathbf{k}}^{x(y)} = 2i t_{dp} \sin \frac{k_{x(y)}}{2}$ and $\zeta_{\mathbf{k}}^p = -4t_{pp} \sin \frac{k_x}{2} \sin \frac{k_y}{2}$, where t_{dp} is the transfer energy between a d -orbital and a neighboring $p^{x(y)}$ -orbital and t_{pp} is that between a p^x -orbital and a p^y -orbital. In this study, we take t_{dp} as the unit of energy. The residual part, H_1 , is described as

$$H_1 = \frac{U}{N} \sum_{\mathbf{k}\mathbf{k}'} \sum_{\mathbf{q}} d_{\mathbf{k}+\mathbf{q}}^\dagger d_{\mathbf{k}'-\mathbf{q}}^\dagger d_{\mathbf{k}'\downarrow} d_{\mathbf{k}\uparrow}. \quad (3)$$

where U is the on-site Coulomb repulsion between d -orbitals and N is the number of \mathbf{k} -space lattice points in the first Brillouin zone (FBZ).

3. UFLEX

We have developed UFLEX in order to analyze the spatially inhomogeneous system. In our UFLEX formulation we introduce 'cluster' momentum besides 'usual' momentum. The notion of this cluster momentum is suggested from the one in dynamical cluster approximation, in which the nonlocal correlations are considered beyond dynamical mean field theory.¹⁹⁻²¹

However, our cluster momentum is not directly related with a coarse graining of the Brillouin zone. When the most stable state of our system is spatially homogeneous, only a cluster momentum, $\mathbf{K} = \mathbf{0}$, is enough to obtain the *true* solution for our problem. In that case, UFLEX is consistent to 'usual' FLEX.¹⁸ The advantage of our introduction of cluster momenta is its flexibility in the correspondence to the problem. If the problem have some important classes of the spatial inhomogeneities, we will only need to provide the cluster momenta corresponding to those classes. For example, when the most important instability is the anti-ferromagnetic one, two cluster momenta, $\mathbf{K} = \mathbf{0}$ and $\mathbf{K} = (\frac{\pi}{2}, \frac{\pi}{2})$, are enough. Of course, the stripe instabilities have their characteristic cluster momenta. Thus, when we anticipate to encounter the stripe instabilities in our problem, we need to provide only those cluster momenta.

First, we define the unrestricted perturbed Green function, $G_{d\mathbf{K}}^\sigma(\mathbf{k}, i\epsilon_n)$. Here we use the abbreviation of Fermion Matsubara frequencies, $\epsilon_n = \pi T(2n + 1)$ with integer n , where T

is the temperature. \mathbf{K} indicates the cluster momentum. The set, $\{\mathbf{K}\}$, is chosen so that any sum, $\mathbf{k} + \mathbf{K}$, exists in the set, $\{\mathbf{k}\}$. $G_{d\mathbf{K}}^\sigma(\mathbf{k}, i\epsilon_n)$ is calculated by the Dyson equation :

$$[G_{d\mathbf{K}}^\sigma(\mathbf{k}, i\epsilon_n)]^{-1} = \delta_{\mathbf{K}} \cdot \left\{ G_d^{\sigma(0)}(\mathbf{k}, i\epsilon_n) \right\}^{-1} - \Sigma_{\mathbf{K}}^\sigma(\mathbf{k}, i\epsilon_n), \quad (4)$$

where $\delta_{\mathbf{K}}$ means Kronecker's delta, i.e. $\delta_{\mathbf{K}=\mathbf{0}} = 1$ and $\delta_{\mathbf{K}\neq\mathbf{0}} = 0$. $[\dots]^{-1}$ indicates the inverse operation defined so as to satisfy the identity :

$$\delta_{\mathbf{K}} = \sum_{\mathbf{K}'} G_{d\mathbf{K}-\mathbf{K}'}^\sigma(\mathbf{k} + \mathbf{K}' - \mathbf{K}, i\epsilon_n) [G_{d\mathbf{K}'}^\sigma(\mathbf{k}, i\epsilon_n)]^{-1} \quad (5)$$

for all \mathbf{k} and n . $G_d^{\sigma(0)}(\mathbf{k}, i\epsilon_n)$ in Eq. (4) is the unperturbed Green function derived by diagonalizing of $H - H_1$ as

$$\left\{ G_d^{\sigma(0)}(\mathbf{k}, z - \mu) \right\}^{-1} = z - \Delta_{dp} - \frac{2z(2 - \cos k_x - \cos k_y) + 8t_{pp}(1 - \cos k_x)(1 - \cos k_y)}{z^2 - 4t_{pp}^2(1 - \cos k_x)(1 - \cos k_y)}. \quad (6)$$

In order to estimate our unrestricted self-energy, $\Sigma_{\mathbf{K}}^\sigma(\mathbf{k}, i\epsilon_n)$, in Eq. (4), we adopt the UFLEX as follows.

$$\begin{aligned} \Sigma_{\mathbf{K}}^\sigma(\mathbf{k}, i\epsilon_n) = & \frac{TU}{N} \sum_{\mathbf{q}n'} G_{d\mathbf{K}}^{-\sigma}(\mathbf{k} - \mathbf{q}, i\epsilon_{n'}) e^{i\epsilon_{n'}\eta} \Big|_{\eta \rightarrow +0} \\ & + \frac{T}{N} \sum_{\mathbf{q}\mathbf{K}'m} G_{d\mathbf{K}-\mathbf{K}'}^\sigma(\mathbf{q} - \mathbf{k} + \mathbf{K}' - \mathbf{K}, i\omega_m - i\epsilon_n) V_{\mathbf{K}'}^{(\text{pp})}(\mathbf{q}, i\omega_m) \\ & + \frac{T}{N} \sum_{\mathbf{q}\mathbf{K}'m} \left[G_{d\mathbf{K}-\mathbf{K}'}^{-\sigma}(\mathbf{k} - \mathbf{q}, i\epsilon_n - i\omega_m) V_{\mathbf{K}'}^{\sigma(\text{ph1})}(\mathbf{q}, i\omega_m) \right. \\ & \left. + G_{d\mathbf{K}-\mathbf{K}'}^\sigma(\mathbf{k} - \mathbf{q}, i\epsilon_n - i\omega_m) V_{\mathbf{K}'}^{\sigma(\text{ph2})}(\mathbf{q}, i\omega_m) \right], \end{aligned} \quad (7)$$

$$\begin{aligned} V_{\mathbf{K}}^{(\text{pp})}(\mathbf{q}, i\omega_m) = & U^2 \phi_{\mathbf{K}}(\mathbf{q}, i\omega_m) \\ & - U^2 \sum_{\mathbf{K}'} \phi_{\mathbf{K}-\mathbf{K}'}(\mathbf{q}, i\omega_m) \left[\delta_{\mathbf{K}'} + U \phi_{\mathbf{K}'}(\mathbf{q} + \mathbf{K} - \mathbf{K}', i\omega_m) \right]^{-1}, \end{aligned} \quad (8)$$

$$\begin{aligned} V_{\mathbf{K}}^{\sigma(\text{ph1})}(\mathbf{q}, i\omega_m) = & - U^2 \chi_{\mathbf{K}}^{\sigma-\sigma}(\mathbf{q}, i\omega_m) \\ & + U^2 \sum_{\mathbf{K}'} \chi_{\mathbf{K}-\mathbf{K}'}^{\sigma-\sigma}(\mathbf{q}, i\omega_m) \left[\delta_{\mathbf{K}'} - U \chi_{\mathbf{K}'}^{\sigma-\sigma}(\mathbf{q} + \mathbf{K} - \mathbf{K}', i\omega_m) \right]^{-1}, \end{aligned} \quad (9)$$

and

$$\begin{aligned}
V_{\mathbf{K}}^{\sigma(\text{ph}2)}(\mathbf{q}, i\omega_m) = & \\
U^2 \sum_{\mathbf{K}'} \chi_{\mathbf{K}-\mathbf{K}'}^{-\sigma-\sigma}(\mathbf{q}, i\omega_m) & \\
\times [\delta_{\mathbf{K}'} - U^2 \sum_{\mathbf{K}''} \chi_{\mathbf{K}'-\mathbf{K}''}^{\sigma\sigma}(\mathbf{q} + \mathbf{K} - \mathbf{K}', i\omega_m) & \\
\times \chi_{\mathbf{K}''}^{-\sigma-\sigma}(\mathbf{q} + \mathbf{K} - \mathbf{K}'', i\omega_m)]^{-1}, & \quad (10)
\end{aligned}$$

where $\omega_m = 2m\pi T$ with integer m are Boson Matsubara frequencies,

$$\begin{aligned}
\phi_{\mathbf{K}}(\mathbf{q}, i\omega_m) = & \\
\frac{T}{N} \sum_{\mathbf{k}\mathbf{K}'n} G_{d\mathbf{K}-\mathbf{K}'}^{\sigma}(\mathbf{q} - \mathbf{k}, i\omega_m - i\epsilon_n) G_{d\mathbf{K}'}^{-\sigma}(\mathbf{k}, i\epsilon_n), & \quad (11)
\end{aligned}$$

and

$$\begin{aligned}
\chi_{\mathbf{K}}^{\sigma\sigma'}(\mathbf{q}, i\omega_m) = & \\
-\frac{T}{N} \sum_{\mathbf{k}\mathbf{K}'n} G_{d\mathbf{K}-\mathbf{K}'}^{\sigma}(\mathbf{q} + \mathbf{k}, i\omega_m + i\epsilon_n) G_{d\mathbf{K}'}^{\sigma'}(\mathbf{k} - \mathbf{K}', i\epsilon_n). & \quad (12)
\end{aligned}$$

In order to obtain the solution satisfying the conserving law, we need to solve Eqs. (4,7,8,9,10,11, 12) fully self-consistently. This self-consistent procedure is shown in Fig. 1 diagrammatically.

In numerical calculations we divide the FBZ into 16×16 meshes. We take 8×8 cluster momenta so that we can reproduce a homogeneous state, inhomogeneous states with 2-, 4-, or 8-lattice period charge density wave (CDW) or spin density wave (SDW) along $a(x)$ -axis or $b(y)$ -axis, or an AF state. We prepare $2^{11} = 2048$ Matsubara frequencies for temperature $T = 0.020 \sim 180\text{K}$. The other parameters : $t_{dp} = 1.0 \sim 0.80\text{eV}$, $t_{pp} = 0.60 \sim 0.48\text{eV}$, and $\Delta_{dp} = 0.70 \sim 0.56\text{eV}$, $U = 4.0 \sim 3.2\text{eV}$, which are all common for our results.

4. Fermi surface evolution with hole- or electron-doping

We have obtained the fully self-consistent solutions for $0.000 \leq \delta_{\text{h}} \leq 0.057$, $0.112 \leq \delta_{\text{h}} \leq 0.231$, and $0.000 \leq \delta_{\text{e}} \leq 0.249$, where $\delta_{\text{h}} \equiv 1 - n_{\text{d}} - n_{\text{p}}$ and $\delta_{\text{e}} \equiv n_{\text{d}} + n_{\text{p}} - 1$. n_{d} and n_{p} represent the number of d - and p -electrons, respectively. We could not obtain any convergent solution for $0.057 < \delta_{\text{h}} < 0.112$. According to the elaborated neutron scattering experiments on $\text{La}_{2-x-y}\text{Ba}_x\text{Sr}_y\text{CuO}_4$,²²⁻²⁴ in this region the inhomogeneous states with longer than 8-lattice period SDW along diagonal, which is called diagonal stripe state, could be realized. Our present calculation would be short of provided cluster momenta to reproduce the inhomogeneous states with the diagonal fluctuations. Hereafter, we restrict our discussion to the states with the vertical fluctuations.

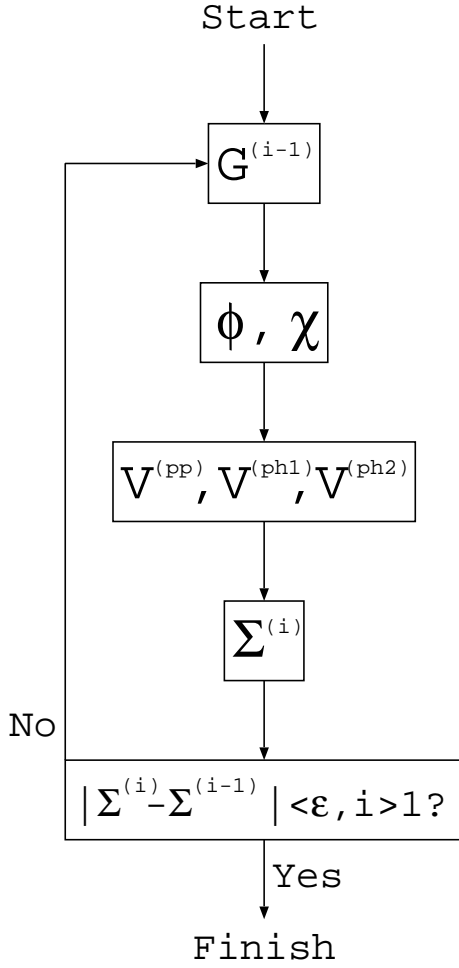


Fig. 1. The self-consistent procedure in UFLEX. i represents the iteration count, and ε is the small value.

In this section we investigate the Fermi surface evolution with doping in detail. In order to determine the Fermi surface, we define the one-particle spectral weight as

$$A^\sigma(\mathbf{k}, E) \equiv -\frac{1}{\pi} \text{Im} \sum_{\zeta=d, p^x, p^y} G_{\zeta\mathbf{0}}^\sigma(\mathbf{k}, i\epsilon_n) \Big|_{i\epsilon_n \rightarrow E}, \quad (13)$$

where

$$\begin{aligned} & G_{p^x, y\mathbf{0}}^\sigma(\mathbf{k}, z - \mu) \\ &= \{z[z - \Delta_{dp} - \Sigma_{\mathbf{0}}^\sigma(\mathbf{k}, z)] - 2(1 - \cos k_{x,y})\} \\ & \quad \times \{[z^2 - 4t_{pp}^2(1 - \cos k_x)(1 - \cos k_y)][z - \Delta_{dp} - \Sigma_{\mathbf{0}}^\sigma(\mathbf{k}, z)] \\ & \quad - 2z(2 - \cos k_x - \cos k_y) - 8t_{pp}(1 - \cos k_x)(1 - \cos k_y)\}^{-1}. \end{aligned} \quad (14)$$

In Eq. (13) we use Padé approximation for the method of analytic continuation. In order to determine the Fermi surface on the basis of our calculated results, we should calculate the one

particle spectral weight at $E = 0$, $A^\sigma(\mathbf{k}, 0)$, and find the \mathbf{k} -points at which $A^\sigma(\mathbf{k}, 0)$ becomes large. Because the thermal fluctuation with CDW, SDW, or anti-ferromagnetic instabilities can generate the branched energy dispersion, we show our calculated results as follows. We choose the both \mathbf{k} -points on which the one-particle spectral weight at $E = 0$ has the largest and the second largest peaks for fixed k_x as far as $0 < k_y \leq k_x < \pi$. And we repeat this operation for the other parts of FBZ. In the following figures, the points on which the one-particle spectral weight at $E = 0$ has the largest and the second largest peaks are to be indicated with black and gray circles, respectively. Our results have been obtained at high temperature, and the thermal fluctuations make the Fermi level vague. However, if we have empty spaces surrounded by these points, we can expect the branched energy dispersion near the Fermi level. The branched energy dispersion is made by a spatial inhomogeneous instability. Furthermore, these points can suggest the Fermi surface connectivities at lower temperature.

Firstly, we should mention our results for the hole-doped states around 1/8-filling, in which the dynamical stripe state might be realized. As shown in Fig. 2, near 1/8-filling we have eight empty spots around the intersections of the planes indicated by dashed and dotted lines, which relate to the anti-ferromagnetic and the 4-lattice period CDW instabilities, respectively. It means that the one-particle spectral weights are lost due to the fluctuations both of the anti-ferromagnetic instability and of the 4-lattice period CDW instability. These instabilities occur when some parts of the Fermi surface are connected with one another by the nesting vectors. The parts of Fermi surface connected with one another by the nesting vectors, (π, π) or $(\pi, -\pi)$, are called 'hot spots'. On hot spots the quasi-particles play important roles in the transport phenomena. Therefore, we expect some anomalous electronic behaviors near 1/8-filling, when the one-particle spectral weights are lost on hot spots. This is the reason why so-called 1/8-problem occurs around 1/8-filling.

Secondly, we show our results for lightly-hole-doped states, in which the anti-ferromagnetic instability might exist. In this case we have no more eight empty spots but four empty spots centered on $(\pm\pi/2, \pm\pi/2)$ as shown in Fig. 3. These empty spots are called 'Fermi arc's, which is believed to appear when the strong anti-ferromagnetic fluctuation exists. In fact, these Fermi arcs have been observed in $\text{La}_{1.97}\text{Sr}_{0.03}\text{CuO}_4$ by ARPES and interpreted as the evidence of the anti-ferromagnetic long-range order.²⁵ In our calculating results, the spectral weights in these Fermi arcs are not completely zero, and the anti-ferromagnetic long-range order does not exist. However, the existence of these Fermi arcs should be originated from the strong anti-ferromagnetic fluctuation, evolving toward the anti-ferromagnetic long-range order.

When the doped holes become less, electrons should localize due to strong coulomb repulsion among them in real materials. However, in our three-band Hubbard model electrons

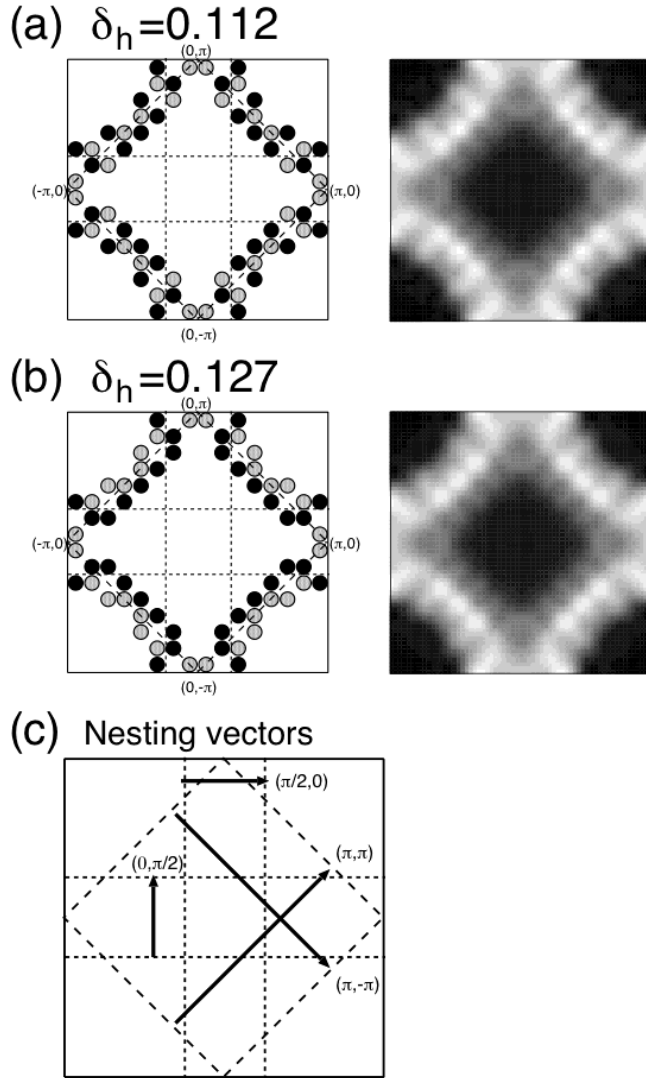


Fig. 2. Fermi surface evolutions near 1/8-filling. Left sides : (a) for $\delta_h = 0.112$. (b) for $\delta_h = 0.127$. Right sides : The gray-scale images interpolated from raw data are attached on account of the guide to the eye. The brighter spots have the larger spectral weights. (c) Illustration of nesting vectors. Dashed lines represent the planes connected with one another by the nesting vectors, (π, π) or $(\pi, -\pi)$. Dotted lines represent the planes connected with one another by the nesting vectors, $(\pi/2, 0)$ or $(0, \pi/2)$. The illustration of nesting vectors is also applicable to the other figures representing Fermi surface evolutions.

cannot localize even around near half-filling and the Fermi surface are remained, as shown in Fig. 4. If we could reproduce the Fermi surface evolution for the whole doping region, the one electron spectral weight at the Fermi level should be almost vanished near half-filling. This result means that our formulation on the basis of UFLEX is not efficient to describe the Mott-Hubbard metal-insulator transition. Unfortunately this is the side-effect of UFLEX, in which we overestimate the thermal fluctuations and recover the itinerancy of electrons.

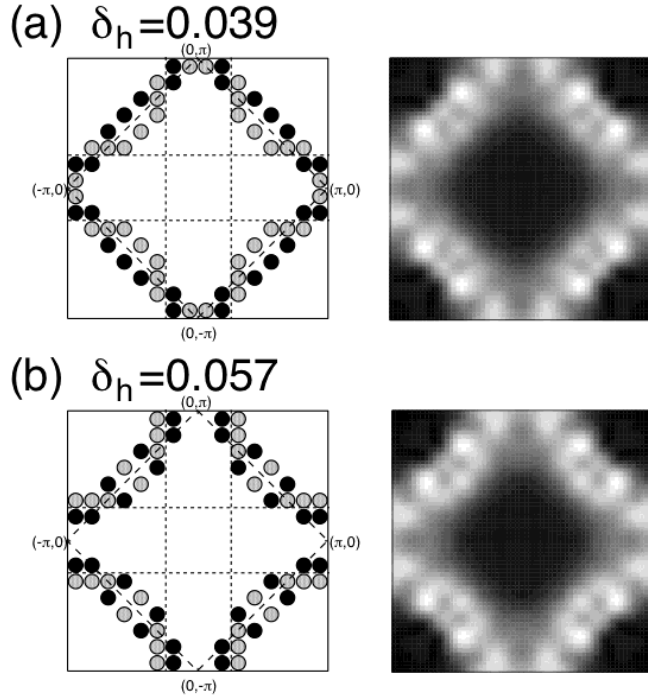


Fig. 3. Fermi surface evolutions for lightly-hole-doped states. (a) for $\delta_h = 0.039$. (b) for $\delta_h = 0.057$.

It would be our future issue to describe the localized electrons but with strong fluctuations appropriately.

Our results for electron-doped states will be highlighted. The ARPES have already clarified the doping dependence of the Fermi surface in $\text{Nd}_{2-x}\text{Ce}_x\text{CuO}_{4\pm\delta}$.^{26–28} Except for completely vanished Fermi surface near half-filling, their observed evolution of Fermi surface with electron doping are consistent with our calculated result. As shown in Fig. 5, in lightly-electron-doped region the eight pockets emerge around the cross-sectional point of Fermi surface with FBZ boundaries. This reflects that the vertical charge fluctuation exists in the lightly-electron-doped region as well as near 1/8-hole-doped region. We can guess that the vertical charge fluctuation gets to play an important role when the localized electron recovers its itinerancy as doped electron increases. When the doped-electron density increases more, each two of eight pockets on the same Fermi surface section come close to each other and unite into one as shown in Fig. 6. Thus, in heavily-electron-doped region we have four pockets around the cross-sectional point of Fermi surface with $k_x = \pm k_y$. This means that the diagonal spin fluctuation, which is not completely anti-ferromagnetic, is strengthened instead of the vertical fluctuation. This diagonal spin fluctuation can cause pseudo-gap phenomena in electron-doped high- T_c as observed at low temperature.²⁹ It contrasts with the case of the hole-doped region, and the difference should be caused by both a large t_{pp} . Such a t_{pp} makes the big difference of the energy dispersions between the hole-doped region and the electron-doped region. If

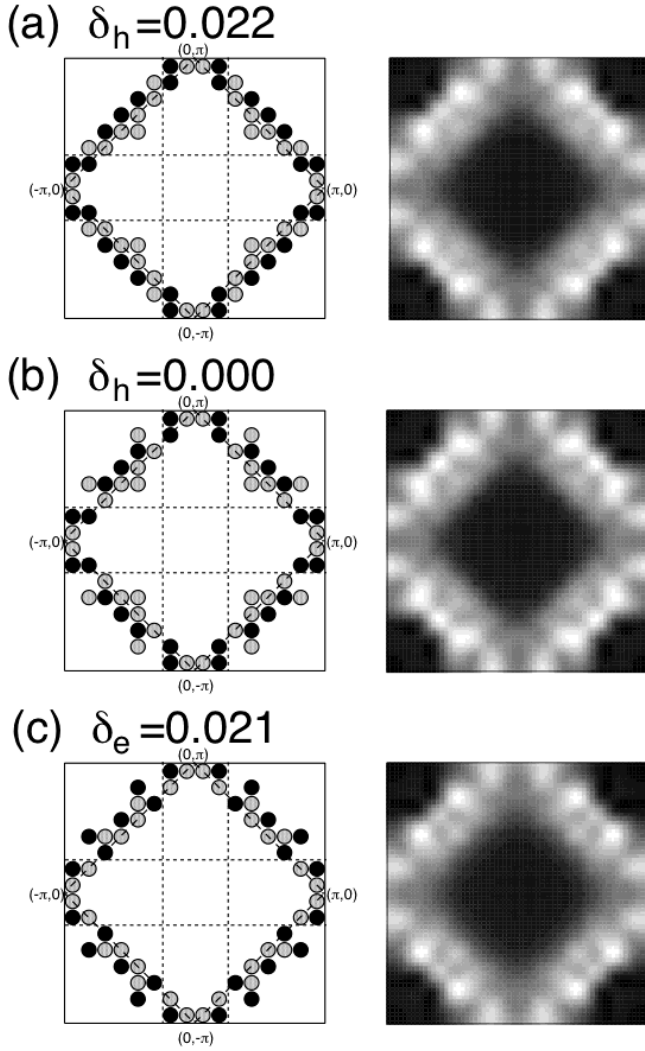


Fig. 4. Fermi surface evolutions for near half-filling. (a) for $\delta_h = 0.022$. (b) for half-filling. (b) for $\delta_e = 0.021$.

the electron were localized, the difference of the energy dispersions should appear as the different charge distributions. In our results the electron could not be localized, but the charge fluctuations appear in the different way between the hole-doped region and the electron-doped region instead. Hence, we can insist that the inhomogeneity of the strongly correlated system should be considered.

5. Spin and charge correlations

In this section we show how the Fermi surface evolution with doping is related to the development of the spin and charge correlations. The momentum dependences of spin and charge correlation functions reflect the spin and charge spatial inhomogeneities, respectively.

At first we sum up our obtained results about the static spin correlations as both the incommensurabilities and the intensities of the peaks in the calculated elastic neutron scattering.

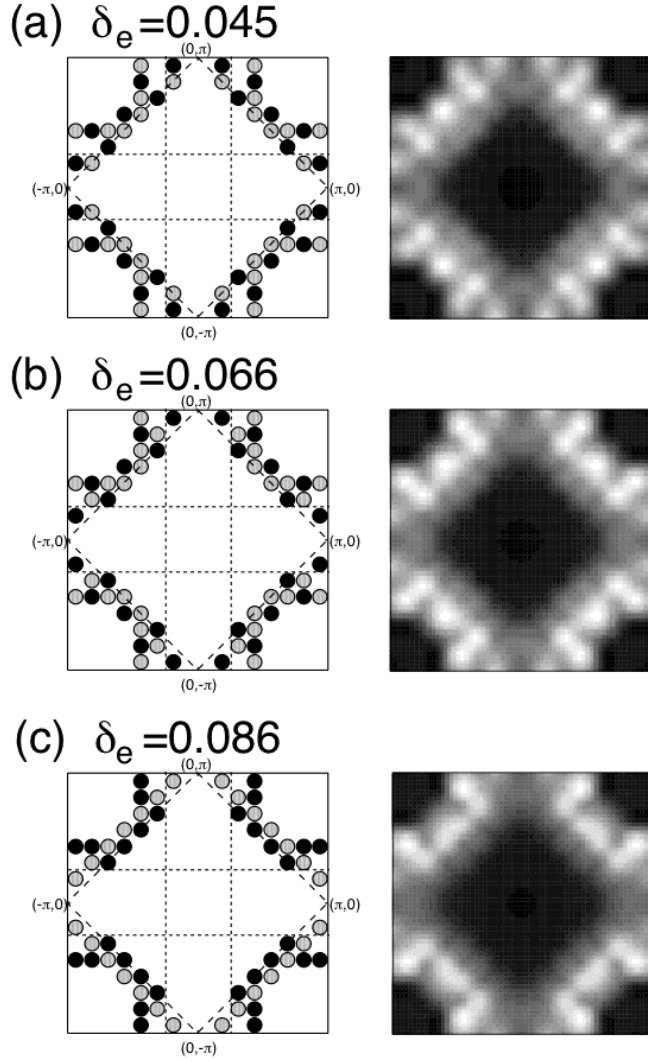


Fig. 5. Fermi surface evolutions for lightly-electron-doped states. (a) for $\delta_e = 0.045$. (b) for $\delta_e = 0.066$. (c) for $\delta_e = 0.086$.

They are shown in Fig. 7, where

$$S(\mathbf{q}) \equiv \sum_{\mathbf{K}} \chi_{-\mathbf{K}}^{+-}(\mathbf{q}, 0) [\delta_{\mathbf{K}} - U \chi_{\mathbf{K}}^{+-}(\mathbf{q} - \mathbf{K}, 0)]^{-1}. \quad (15)$$

In the hole-doped region the incommensurabilities δ_{inc} , defined by

$$\delta_{\text{inc}} \equiv \text{Max}\{[\mathbf{Q}_{\text{max}} - (\pi, \pi)]_x, [\mathbf{Q}_{\text{max}} - (\pi, \pi)]_y\}, \quad (16)$$

are almost proportional to δ_h . This has been already observed by the neutron scattering experiment on $\text{La}_{2-x-y}\text{Ba}_x\text{Sr}_y\text{CuO}_4$.^{22,23,30} The ratio of δ_{inc} to δ_h in our calculating results are almost half of the one in these experiments. However, we believe that this deviation is originated from the difference between the real hole number δ_h introduced in CuO_2 plane, which is correspond to the one in our results, and the instoicheiometric number δ used in the analysis in Ref. 30.

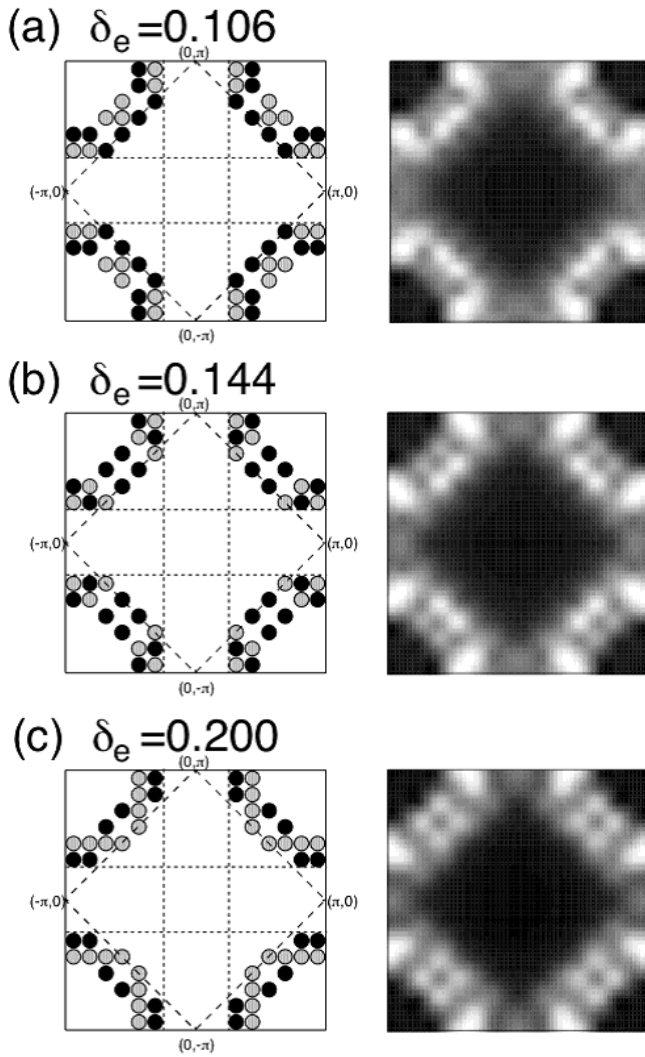


Fig. 6. Fermi surface evolutions for heavily-electron-doped states. (a) for $\delta_e = 0.106$. (b) for $\delta_e = 0.144$. (c) for $\delta_e = 0.200$.

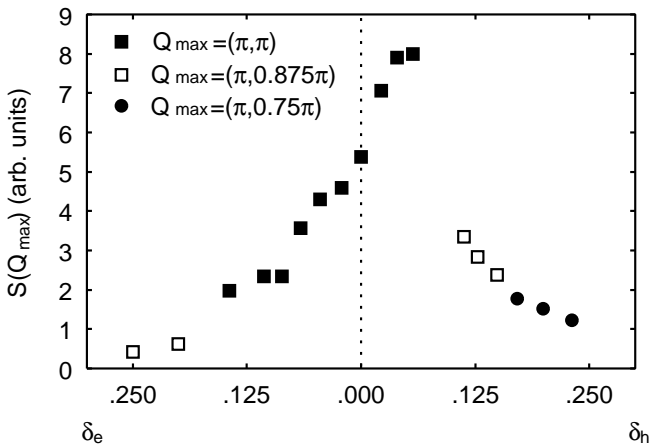


Fig. 7. The doping dependence of $S(\mathbf{q})$ at its maximum momentum \mathbf{Q}_{\max} .

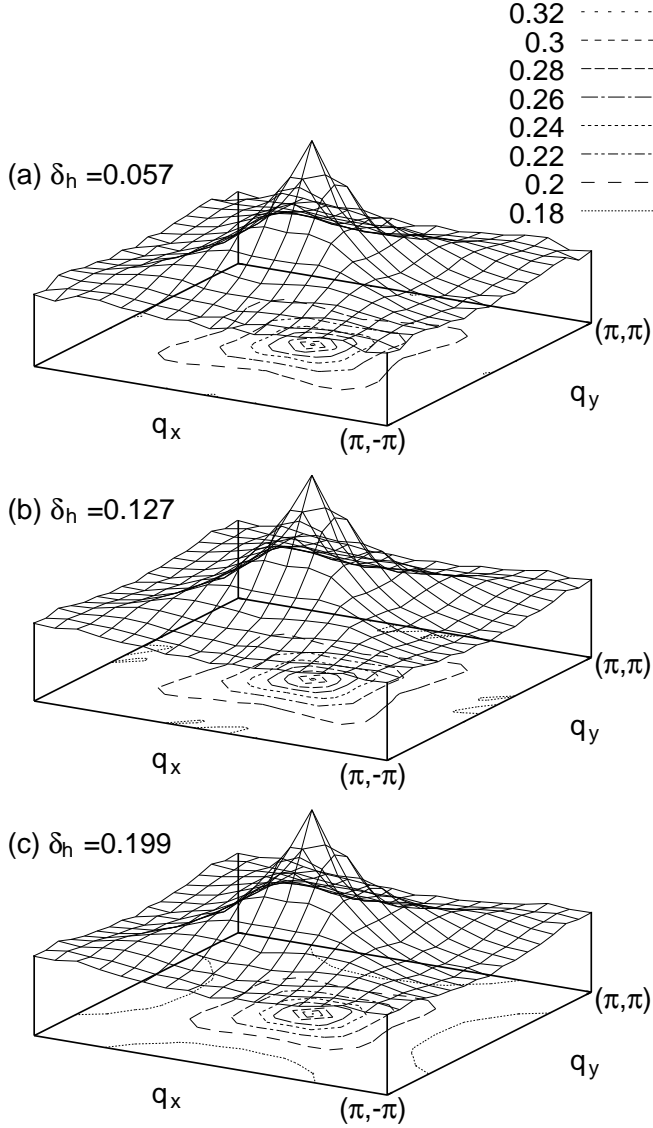


Fig. 8. The momentum dependences of $D(\mathbf{q})$ at hole-doped regions.

On the other hand, in the electron-doped region we cannot recognize such a relationship between δ_{inc} and δ_e . It suggests that our spin correlation functions do not simply reflect the Fermi surface nesting but rather the existence of inhomogeneities as discussed in Section 4.

In order to clear our insistence, we calculate the static charge correlation functions at some regions. The momentum dependences of these correlation functions are shown in Figs. 8 and 9, where

$$D(\mathbf{q}) \equiv \frac{T}{N} \sum_{\mathbf{k}\mathbf{K}'n} G_{d\mathbf{K}'}^{\sigma}(\mathbf{q} - \mathbf{k}, -i\epsilon_n) G_{d-\mathbf{K}'}^{-\sigma}(\mathbf{k}, i\epsilon_n). \quad (17)$$

Focusing on Fig. 8(b) and Fig. 9(b), we can recognize that $D(\mathbf{q})$ are slightly enhanced around the symmetric lines, $q_x = 0$ and $q_y = 0$. These momentum dependences of $D(\mathbf{q})$ suggest that the two collective modes with the momenta $(\pm 1, 0)$ and $(0, \pm 1)$ exist. These collective modes

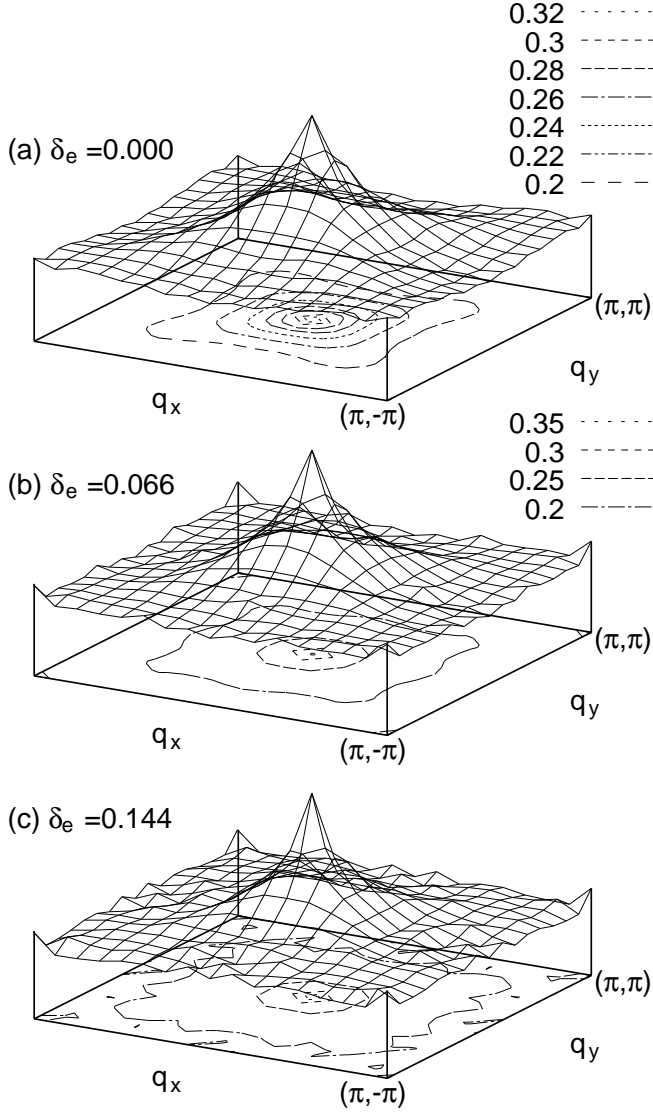


Fig. 9. The momentum dependences of $D(\mathbf{q})$ at electron-doped regions.

can be translated as the instabilities toward vertical charge orderings along x -axis and y -axis, respectively. In fact, when $\delta_h = 0.127$ and $\delta_e = 0.066$, the Fermi surfaces have eight pockets around $(\pm\pi, \pm\pi/4)$ and $(\pm\pi/4, \pm\pi)$ as shown in Fig. 2(b) and Fig. 4(b), respectively. As discussed in 4, these anomalous Fermi surfaces are caused from the charge inhomogeneities, which appear as shown in Fig. 8(b) and Fig. 9(b).

6. Conclusion

In this paper, we have obtained fully self-consistent solutions for the 2D three-band Hubbard model on the basis of UFLEX, in which the inhomogeneous distribution of d -electrons are allowed. Both in hole-under-doped and electron-doped regions the one-particle spectral weights behave anomalously. Furthermore, the spin and charge correlation functions reflect

the existence of super-lattice structures around $1/8$ -filling. Our numerical solutions show that the metallic state with spatially inhomogeneous spin or charge fast fluctuation can exist at high-temperature. The electronic state in one of our microscopically derived solutions corresponds to the dynamical stripe state mentioned in some pioneering works.^{14–17} In our 2D model, the electrons cannot have the long-range order at finite temperature because of the strong fluctuation characteristic of low-dimensionality. However, in three-dimensional real materials, the spatially inhomogeneous fluctuation may tend to have the long-range order and form the striped state, observed in the neutron scattering experiments. This long-range order formation in three-dimensional real materials might not be reproduced by our simple model in this paper. The existences of the phonon or the long-range Coulomb potential might have an important role for these long-range order formation. The theoretical researches concerning these complicated factors are to be expected as the future problem.

Acknowledgments

The authors are grateful to Professor K. Yamaji, Professor Y. Aiura, Professor H. Eisaki, Dr. I. Nagai, Dr. M. Miyazaki, and Dr. S. Koike for their invaluable comments. The computation in this work has been done using the facilities of the Supercomputer Center, Institute for Solid State Physics, University of Tokyo. The early development of the code for this computation has been achieved by using the IBM RS/6000-SP at TACC and VT-Alpha servers at NeRI in AIST.

References

- 1) J. M. Tranquada, B. J. Sternlieb, J. D. Axe, Y. Nakamura, and S. Uchida: *Nature* **375** (1995) 561.
- 2) S. R. White and D. J. Scalapino: *Phys. Rev. Lett.* **80** (1998) 1272.
- 3) D. Poilblanc and T. M. Rice: *Phys. Rev. B* **39** (1989) R9749.
- 4) J. Zaanen and O. Gunnarsson: *Phys. Rev. B* **40** (1989) R7391.
- 5) M. Kato, K. Machida, H. Nakanishi, and M. Fujita: *J. Phys. Soc. Jpn.* **59** (1990) 1047.
- 6) T. Mizokawa and A. Fujimori: *Phys. Rev. B* **56** (1997) 11920.
- 7) M. Ichioka and K. Machida: *J. Phys. Soc. Jpn.* **68** (1999) 4020.
- 8) T. Yanagisawa et al., *J. Phys.: Condens. Matter* **14** (2002) 21.
- 9) M. I. Salkola, V. J. Emery, and S. A. Kivelson: *Phys. Rev. Lett.* **77** (1996) 155.
- 10) K. Machida and M. Ichioka: *J. Phys. Soc. Jpn.* **68** (1999) 2168.
- 11) E. Kaneshita, M. Ichioka, and K. Machida: *J. Phys. Soc. Jpn.* **70** (2001) 866.
- 12) S. Varlamov and G. Seibold: *Phys. Rev. B* **65** (2002) 075109.
- 13) J. M. Tranquada, N. Ichikawa, and S. Uchida: *Phys. Rev. B* **59** (1999) 14712.
- 14) J. Zaanen and A. M. Ole's: *Ann. Physik* **5** (1996) 224.
- 15) J. Zaanen: *Nature* **404** (2000) 714.
- 16) J. Zaanen: *Nature* **422** (2003) 569.
- 17) N. Hasselmann, A. H. Castro Neto, and C. M. Smith: *Phys. Rev. B* **65** (2002) 220511(R).
- 18) N. E. Bickers and D. J. Scalapino: *Ann. Phys.* **193** (1989) 206.
- 19) M. H. Hettler, A. N. Tahvildar-Zadeh, M. Jarrell, T. Pruschke, and H. R. Krishnamurthy: *Phys. Rev. B* **58** (1998) R7475.
- 20) Th. Maier, M. Jarrell, Th. Pruschke, and J. Keller: *Eur. Phys. J. B* **13** (2000) 613.
- 21) Y. Imai and N. Kawakami: *Phys. Rev. B* **65** (2002) 233103.
- 22) M. Fujita, H. Goka, K. Yamada, and M. Matsuda: *Phys. Rev. B* **66** (2002) 184503.
- 23) M. Fujita, H. Goka, K. Yamada, and M. Matsuda: *Phys. Rev. Lett.* **88** (2002) 167008.
- 24) J. M. Tranquada, H. Woo, T. G. Perring, H. Goka, G. D. Gu, G. Xu, M. Fujita, and K. Yamada: *Nature* **429** (2004) 534.
- 25) T. Yoshida, X. J. Zhou, T. Sasagawa, W. L. Yang, P. V. Bogdanov, A. Lanzara, Z. Hussain, T. Mizokawa, A. Fujimori, H. Eisaki, Z.-X. Shen, T. Kakeshita, and S. Uchida: *Phys. Rev. Lett.* **91** (2003) 027001.
- 26) N. P. Armitage, F. Ronning, D. H. Lu, C. Kim, A. Damascelli, K. M. Shen, D. L. Feng, H. Eisaki, Z.-X. Shen, P. K. Mang, N. Kaneko, M. Greven, Y. Onose, Y. Taguchi, and Y. Tokura: *Phys. Rev. Lett.* **88** (2002) 257001.
- 27) N. P. Armitage, D. H. Lu, C. Kim, A. Damascelli, K. M. Shen, F. Ronning, D. L. Feng, P. Bogdanov, X. J. Zhou, W. L. Yang, Z. Hussain, P. K. Mang, N. Kaneko, M. Greven, Y. Onose, Y. Taguchi, Y. Tokura, and Z.-X. Shen: *Phys. Rev. B* **68** (2003) 064517.
- 28) K. M. Shen, T. Yoshida, D. H. Lu, F. Ronning, N. P. Armitage, W. S. Lee, X. J. Zhou, A. Damascelli, D. L. Feng, N. J. C. Ingle, H. Eisaki, Y. Kohsaka, H. Takagi, T. Kakeshita, S. Uchida, P. K. Mang, M. Greven, Y. Onose, Y. Taguchi, Y. Tokura, Seiki Komiya, Yoichi Ando, M. Azuma, M. Takano, A. Fujimori, and Z.-X. Shen: *Phys. Rev. B* **69** (2004) 054503.
- 29) Y. Onose, Y. Taguchi, K. Ishizaka, and Y. Tokura: *Phys. Rev. B* **69** (2004) 024504.
- 30) K. Yamada, C. H. Lee, K. Kurahashi, J. Wada, S. Wakimoto, S. Ueki, H. Kimura, Y. Endoh,

S. Hosoya, G. Shirane, R. J. Birgeneau, M. Greven, M. A. Kastner, and Y. J. Kim: Phys. Rev. B
57 (1998) 6165.